RSC Advances

ROYAL SOCIETY OF CHEMISTRY

www.rsc.org/advances

RSC Advances

RSCPublishing

ARTICLE

Hierarchical Coated Metal Hydroxide Nanoconstructs as Potential Controlled Release Carriers of Photosensitizer for Skin Melanoma †

Cite this: DOI: 10.1039/xoxxoooooox

Received ooth January 20xx,
Accepted ooth January 20xx

DOI: 10.1039/xoxxoooooox

www.rsc.org/

Ranjith Kumar Kankala,[a] Yaswanth Kuthati,[a] Chen-Lun Liu*[a] and Chia-Hung Lee*[a]

Inorganic nanostructured ensembles containing an anionic clay matrix with layered double hydroxide (LDH) specifically were designed in nanooncology for photosensitizer delivery. A strategy of a core-shell phenomenon combined with host guest chemistry by the intercalation of indole-3-acetic acid (IAA). This single formulation with good drug loading percentage and compact liposome coat (LDH-IAA-Lipo) over/around the positively charged layered surface establishes a controlled release property for the treatment of skin melanoma. All the data regarding synthesis, physical characterization, chemical stability by thermogravimetric analysis and the coat stability by leaching test in solvent mixture containing triton X-100 and biological buffer was obtained. IAA was estimated using high-performance liquid chromatography (HPLC) with optimized conditions with the outcome being admirable. Improvement in cytotoxic studies under the visible light exposure has been confirmed by MTT, ROS levels, DNA fragmentation using comet assay and apoptosis by analysis of mitochondrial membrane potential (MMP) using the MitoProbe JC-1 assay. In contrast this formulation depicted cytocompatibility in a normal fibroblast (3T3) cell line. Photodynamic therapy (PDT) can be suggestible for long term therapy since the combinatorial efficiency of drug molecules in addition to light irradiation was dramatically evidenced to treat melanoma effectively.

1. Introduction

Skin melanoma is severe infirmity in the melanocytes which metastasize and leads to malignancy and eventually death. Nevertheless the freckles that lead to skin cancer are in contrast with the moles possibly caused by the UV radiation of sunlight.[1, 2] Recently, photodynamic therapy (PDT) has fascinated researchers as an effective therapy using topically applied drugs (photosensitizers).[3-5] In light irradiation these photosensitizers get activated and output in cells as porphyrin derivatives[6, 7] and reactive oxygen species[8, 9] which play a key role in PDT for treating various malignancies.[10] PDT is now applied to benign skin disorders such as warts, acne and various melanomas.[11] It is more advantageous over conventional treatments like surgery chemotherapy and radiation therapy in most of the cancers since it is very simple, non-invasive and most convenient to the patient[12] and selectively targeted towards localized infections. Drugs like cisplatin[13] and docetaxol[14] are preferred for skin melanoma which causes very serious adverse effects and can be bypassed by means of PDT. These days most of the research is being pursued towards the development of typical photosensitizers for topical and systemic delivery to treat various kinds of infections besides cancer.[15] Suitable formulation is designed to deliver a photosensitizer for its accretion in effective therapy.

Layered double hydroxide (LDH) nanoparticles have been explored widely owing to their biocompatibility[16] as well as biodegradability in the biomedical field for cancer treatment termed as nanooncology.[17] These inorganic layered solids are stable[18] and have an ability to encapsulate or immobilize various bio- and organic molecules in the interlayer space.[19-25] Abundant varieties of metal nanocomposites can also be synthesized using different metals with varying compositions, synthetic preparation routes at different hydrodynamic diameter range (30–100 nm) and encompassing various applications.[17, 20, 26-40] One amongst all the classes of anionic clays, nanocomposites with magnesium and aluminum containing nanohybrids have potential drug delivery applications.[41] These clay materials could be useful to tackle diversified cell lines and helpful in targeted therapy for various tumor

[a]Department of Life Science and Institute of Biotechnology, National Dong Hwa University, Hualien, 974, Taiwan.
* Equal Correspondence E-mail: chlee016@mail.ndhu.edu.tw; E-mail: cliu@mail.ndhu.edu.tw

†Electronic Supplementary Information (ESI) available: Additional figures including TGA curves, Table representing particle size distribution and ζ-potential values, FT-IR spectrum (for leaching study), UV-Vis spectra and sample images and free radical determination (by dichlorofluorescein (DCF) fluorescence). Mitochondria membrane potential images, Light power calculation. See DOI: 10.1039/b000000x

environments.[42-50] In general the tumor environment contains leaky vasculature and high permeability due to the inbuilt property of angiogenesis. These nanomaterials can be effectively targeted to the tumor due to the enhanced permeability and retention (EPR) effect[51] while the greater surface area of LDH plays a crucial role in developing an effective therapeutic strategy in the controlled delivery of photosensitizer.[52-55] LDH nanocontainers are versatile carriers which are more effective in terms of drug delivery compared with other inorganic nanoparticles like mesoporous silica nanoparticles (MSNs) that are poor in biodegradability and encapsulation efficiency.[56] Most of these reports indeed suggest LDH as a major carrier system in nanooncology as far as drug delivery using nanovehicles are concerned.[20, 46, 47, 57-68]

Liposome is selected as a supportive coat, since it is a well-known attractive system for controlled release of various drugs used to treat different infections.[69, 70] In addition, liposomes are biocompatible, versatile and remarkable delivery systems with an enormous number of applications[71] on account of the variability in its composition. Biodegradability as well as the structural and biological properties of a delivery system can significantly decrease drug toxicity[72] and accelerate the dissolution capability of drugs. Although a liposome coating is not that familiar in the delivery of photosensitizers, this coating could represent an advance in encapsulating both hydrophilic as well as lipophilic drugs. Eventually the coated nanohybrid is necessarily required for the controlled delivery[73] of photosensitizer[74, 75] at selective sites from the LDH to improve the therapeutic activity as well as to prop up cell uptake.

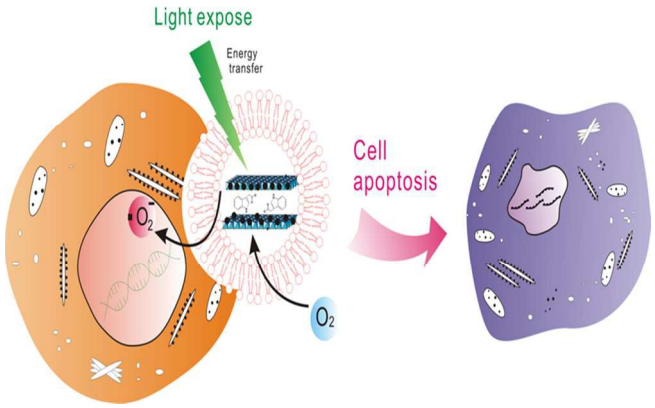

Fig. 1. Schematic representation of the uptake of liposome coated LDH Nanohybrids by cell and resultant apoptosis by photodynamic therapy (PDT)

Indole-3-acetic acid (IAA), a plant hormone has grabbed the attention of researchers since it first activated to produce free radicals when exposed to light at a particular wavelength by the photoactivation process.[76] IAA itself isn't toxic; indeed an agent for PDT resulted in the death of cancer cells by inducing apoptosis in prostate cancer and antimicrobial activity[77] under Ultraviolet-B (UV-B) irradiation.[78] Although previous reports suggest IAA's anti-neoplastic nature is a good example for combinational therapy with the oxidative decarboxylated product of horseradish peroxidase (HRP).[79] However, IAA alone can generate free radicals[80] since the treatment is so effective even at the low oxygen levels common in tumors. It can also be effective at lower light doses than conventional photodynamic therapy,[81] that could act effectively on various cancers.[82-84] We intended to synthesize and formulate a delivery system by encapsulating IAA intercalated LDH (LDH-IAA) within the coat of the liposome layer (LDH-IAA-Lipo) for the controlled delivery of a photosensitizer (Fig. 1). However, this is the first time to report using IAA as a photosensitizer and prove the apoptosis of the skin melanoma cell line under visible light irradiation and its potential of photosensitizing capability measured by optimizing all the conditions.

2. Experimental Section

2.1 Materials

All the reagents, chemicals and organic solvents were of analytical grade at the highest purity and commercially available, and were used without further purification. Indole-3-acetic acid (IAA), Magnesium nitrate hexahydrate [$Mg(NO_3)_2.6H_2O$], Lecithin (phosphatidylcholine), Cholesterol, Ethelenediaminetetraacetic acid (EDTA), were purchased from Alfa Aesar (A Johnson Matthey company, Heysham, England). Aluminium nitrate nonahydrate [$Al(NO_3)_3.9H_2O$], Triton X-100 was obtained from J.T.Baker chemicals Pvt. Ltd (Phillipsburg NJ, USA). Dicetyl phosphate, Sodium phosphate dibasic (Na_2HPO_4), 3-(4,5-dimethylthiazol-2-yl)-2,5-diphenyltetrazolium bromide (MTT), Potassium phosphate monobasic (KH_2PO_4), Potassium phosphate dibasic (K_2HPO_4), Citric acid, n-Butanol, Sodium hydroxide (NaOH), 2',7'-dichlorodihydrofluorescein diacetate (H_2DCFDA), Ninhydrin (2,2-dihydroxyindane-1 ,3-dione), 4',6-Diamidino-2-phenylindole dihydrochloride (DAPI), Formaldehyde (HCHO), Fluorescein isothiocyanate (FITC) were obtained from Sigma. Co. Ltd (St. Louis, MO, USA). Thiobarbituric acid (TBA) was obtained from Acros organics Ltd. Fetal bovine serum (FBS) and Dulbecco's modified Eagle's medium was purchased from GIBCO/BRL Life Technologies (Grand Island, NY, USA). Potassium Bromide (KBr) (FT-IR grade) and (3-Aminopropyl) trimethoxysilane (APTS) were obtained from Fisher scientific ltd (Loughborough, UK) and Gelest (Morrisville, PA, USA) respectively. Rhodium phalloidin was purchased from Invitrogen Ltd (Eugene, Oregon, USA). The comet assay kit was obtained from Trevigen (Gaithersburg, MD, USA).

2.2 Instruments

Centrifugation during the cell culturing process and nanomaterials synthesis was performed at an appropriate temperature using Swing rotor Kubota KN-70 (Tokyo, Japan) and Hermle Z 36 HK (Wehingen, Germany) instruments, respectively. Ultraviolet-visible (UV-Vis) spectroscopic absorbance was recorded on a Genequant-300 series spectrophotometer while fluorescence imaging was captured on an Olympus microscope hybridized with Nikon CCD camera apparatus (Palo Alto, CA, USA) with BD pathway (BD biosciences, USA). 532 nm LED lights purchased locally. B16F10 cell lines were obtained from the Bioresource Collection and Research Center (Hsinchu, Taiwan). Fluorescence intensity and MTT absorbance were recorded using Perkin Elmer's EnSpire Multi-label Plate Reader (Santa Clara California, USA). The flow cytometric

quantification was achieved using a Beckmann Coulter (Cytomics FC-500) equipped with a FSC detection system and argon laser lamp (488 nm emission wavelength) while the date acquisition was in linear mode and the data visualized in logarithmic mode.

2.3 Characterization

Fourier transform infrared (FT-IR) spectra were recorded on a Bruker Alpha spectrometer with a dried KBr pellet. Zeta (ζ)-potential as well as particle size distribution was measured by dynamic light scattering (DLS) (Malvern Nano-HT Zetasizer). The samples were prepared by diluting the nanoparticles suspension with de-ionized water until the counter rate was less than 1.5 Mcps (mega counts per second). The physical state and composition determination of IAA intercalated in the LDH and the strength of liposome coated LDH nanohybrids were investigated by Thermogravimetric analysis-Differential thermal analysis (TGA-DTA) curve on TGA Q50 V20, 13 Build 39 (Universal V4.5A TA Instruments). The temperature increased from ambient to 800 ºC at a rate of 20 ºC /minute under a dry nitrogen purge at a flow rate of 20 mL/min. Powder X-ray diffraction (PXRD) analysis of the samples was carried out using a powder X-ray diffractometer (XRD D8 Advanced, Bruker) to determine the existing nature of IAA in LDH. The diffraction angle (2-theta) was recorded from 20º to 70º with a scanning speed at 3º/minute. CuK_{α} radiation was used as an X-ray source with 40 kilovolts (kV) and 40 milli amperes (mA). Nitrogen adsorption-desorption isotherms were measured by Micrometric ASAP 2010 surface area analyzer at the temperature of liquid nitrogen (-196 ºC) using ultra high purity nitrogen and helium as the adsorbate and carrier gas respectively. For surface area and pore size distribution measurements, about 150 mg of each nanoparticle sample was degassed overnight at 80 ºC under vacuum (10^{-3}Torr). TEM images were captured on a Hitachi H-7100 operating at 100 kV. Samples were prepared by dispersing LDH aqueous solution deposited on carbon coated copper (Cu) grids and dried at room temperature.

2.4 Synthesis of LDH-nanoparticles. Inorganic LDH nanoparticles were synthesized by co-precipitation method as reported previously.[85-87] $Mg(NO_3)_2.6H_2O$ and $Al(NO_3)_3.9H_2O$ (3:1) were dissolved in 10 mL double-distilled water (dd-H_2O) and added instantly to 40 mL of 0.2 M NaOH solution by stirring at room temperature under a nitrogen purge for 10 minutes (min). Atmospheric carbon dioxide (CO_2) entrapment/contamination between the layers was prevented by maintaining an inert atmosphere and by using decarbonated dd-H_2O, accomplished by simultaneous boiling and ultra-sonication. Eventually, the nanoparticles were collected and washed repetitively with 40 mL of dd-H_2O and centrifuged at 13,000 rpm for 15 minutes. The slurry was further suspended in 50 mL dd-H_2O and the solution underwent hydrothermal treatment in a Teflon-lined autoclave at 100 ºC for 16 hours. The nanoparticles were subsequently collected and washed repeatedly by centrifuging at 13,000 rpm for 15 minutes, and finally suspended in ethanol to prevent contamination.

2.5 Synthesis of LDH-IAA nanohybrids. Indole-3-acetic acid (IAA) intercalation was primed using the ion-exchange process as reported previously with slight optimization.[88] We accurately weighed 100 mg of IAA dissolved in 10 mL of water, set to pH 9.0. The nanoparticles then re-suspended in the prepared drug solution at the same ratio and the slurry stirred at 70 ºC for 3 days under a nitrogen atmosphere. Finally, the resultant product was centrifuged and washed repetitively with dd-H_2O and re-suspended in ethanol for further study. This sample was denoted as LDH-IAA (Layered double hydroxide-Indole acetic acid).

2.6 Loading efficiency of IAA in LDH. Quantification of intercalated IAA in LDH nanocontainers was estimated by UV-Vis spectroscopy. Accurately weighed 5 mg of the nanohybrids was placed in 10 mL volumetric flask for which 0.5 mL of 0.1 M hydrochloric acid (HCl) solution was added to mortify LDH, and the rest filled with ethanol. The exact concentration of the drug in solution was determined by monitoring the absorbance at 280 nm (λ_{max}) and the concentration was calculated by regression analysis according to the standard curve obtained from a series of standard solutions of IAA. It was calculated as 19.5% (w/w) of LDH.

2.7 Synthesis of liposome coated LDH nanohybrids. Required amounts of lipid phase with three components lecithin, cholesterol and dicetyl phosphate were weighed and dissolved in chloroform in a molar ratio 7:2:1. Once the lipids were thoroughly mixed in the organic solvent, it was evaporated under reduced pressure at 40 ºC to yield a thin lipid film; this film was dried to remove residual organic solvent by being placed under vacuum overnight. Finally the dried lipid film was hydrated by adding 60 mg of nanoparticles dispersed in 20 mL of the aqueous phase followed by agitation for 1 hour at 45 ºC. Eventually small unilamellar vesicles were prepared by bath sonication for 20 minutes at 45 ºC. This sample was denoted as LDH-IAA-Lipo (Layered double hydroxide-Indole acetic acid-Liposome).

2.8 Synthesis of surface functionalized LDH-FITC. Fluorescein isothiocyanate (FITC) on the surface of LDH was anchored using an amine linker and effectively surface functionalized using toluene as the reaction solvent as reported previously.[89] Since the surface activation of LDH attained at higher temperature is favored by toluene, 0.2 gm of LDH nanoparticle was suspended in 30 mL toluene and stirred vigorously; 1 mL of 97% (3-Aminopropyl) trimethoxysilane (APTS) was added after 30 min to the reaction mixture and stirred for 24 hours at 100 ºC under a nitrogen purge. The resultant nanoparticles were collected and washed repetitively with acetone and ethanol to remove the unconjugated silane. Conjugation was confirmed by the ninhydrin test which is specific to primary amines. FITC was dissolved in dry methanol for successful immobilization of the respective amine on LDH surface. 10 mg of FITC was dissolved in the 10 mL dry methanol and 100 mg of nanoparticles (LDH-NH_2) was re-suspended and stirred for 24 hours in the dark at room temperature. Liposome was coated on the FITC conjugated LDH as mentioned in the above section (Section 2.7).

2.9 Leaching/Stability test. Liposome coat efficiency was measured by performing a leaching test of the liposome coated LDH-IAA (LDH-IAA-Lipo) samples in citrate buffer pH-5.0 with and without triton X-100. This facilitates LDH degradation (only in citrate buffer) and liposome disruption (with triton X-100) respectively. This test directly symbolizes the coat efficiency of liposome around LDH and indirectly represents the IAA intercalation in LDH when treated with the solvent mixture. 10 mg of the respective sample was placed in 200 µL of triton X-100 and the other with a citrate buffer for 30 min while a further 500

µL of citrate buffer was added to both samples and incubated for 4 hours in a rotary shaker at 150 rpm. Finally the supernatant was collected after centrifuging it and analyzed using high-pressure/performance liquid chromatography (HPLC) with the optimized conditions for the detection of IAA.

2.10 HPLC method for IAA determination. IAA detection using HPLC system containing a Hitachi L-2130 HPLC pump attached with a manual injection system and UV detector (Hitachi L-2400) at the specific absorption wavelength of 280 nm. IAA was separated using a Cosmosil C18 column (250 mm×4.6 mm, 5 µm size). Separation was made using the mobile phase with the gradient elution method, beginning with water: acetonitrile (50:50) for the first 8 minutes and the rest with 50:50 acetonitrile: methanol in 15 minutes run. The flow speed maintained of 1.0 mL/min and injection volume fixed at 20 µL.

2.11 *In vitro* drug release study. IAA release study was performed by suspending the LDH-IAA and LDH-IAA-Lipo nanohybrids in phosphate buffer saline (PBS) solutions at various pHs (5.0 and 7.4). The intention is to simulate the passage and mimic the release behavior in different gastrointestinal environments for the purpose of establishing the *in vitro-in vivo* correlation. LDH-IAA-Lipo nanohybrids were additionally ensured in a pH-1.2 (0.1M HCl) buffer at 37 ºC while being stirred at 100 rpm and was continued by replacing the respective simulated fluids at relevant time intervals. Aliquots were removed by centrifuging at 12,000 rpm for 10 minutes and analyzed at 280 nm while the same volume of fresh buffer was replaced for further time hiatus. The released percentage of the drug was determined by measuring the concentration periodically using UV-Vis spectroscopy.

2.12 Cancer studies. To determine the photodynamic therapy using IAA, B16F10 skin melanoma model cell line was used selectivity towards topical delivery for PDT. B16F10 (Mouse melanoma cell line) and normal fibroblast (3T3) cell line were cultured in a Dulbecco's Modified Eagle Medium (DMEM) supplemented with 10% (v/v) fetal bovine serum and penicillin (100 units/mL)/streptomycin (100 µg/mL). Cultures were maintained in a humidified incubator at 37 °C in 5% CO_2.

2.13 Cell viability assay (MTT). Cellular viability was measured using MTT assay which was reported previously.[90] Cells were inoculated into 96 well plates at a density of $1x10^4$ cells per well and incubated for cell attachment. After 24 hours they were subjected with various concentrations in B16F10 cell line (0-250 µg/mL) and 3T3 cell line (0-500 µg/mL) of LDH, LDH-IAA and LDH-IAA-Lipo samples in FBS free DMEM. They were further incubated for 4 hours to facilitate particle uptake and the delivery of photosensitizer; then the light was irradiated for the prescribed time with 532 nm LED green light (Power/cm^2 calculation, see ESI †) and incubated for another 20 hours. At the end of incubation, 50 µL of MTT solution (1 mg/mL of MTT in PBS) was added and further incubated for 4 hours. Finally, the medium was pipetted out and the violet crystals (formazan) were dissolved with 150 µL of dimethyl sulfoxide (DMSO) and the reduction of MTT by mitochondrial dehydrogenase was measured at 570 nm using ELISA reader. In addition, cells without nanoparticle suspension were taken as the control with the viability set as 100%. The percentage viable cells in each well were calculated from the absorbance of purple colored formazan crystals. The final report data was expressed as a percentage of the control (mean±SD). The percentage inhibition of each compound was calculated using the following formula: % inhibition = (Mean absorbance of treated cells/ Mean absorbance of control) x 100.

2.14 Free radical determination. *In vitro* free radical quench by IAA loaded LDH nanohybrids was precisely quantified using 2',7'-dichlorodihydrofluorescein-diacetate (H_2DCF-DA) assay, with the fluorescence measurement taken after the H_2DCF-DA gets oxidized to fluorescent DCF underneath photo irradiation, as reported previously.[78] Prior to the free radical determination, H_2DCF-DA (1mM) was activated using an ethanolic stock solution mixed with 0.01 M NaOH and the resulting reaction mixtures containing nanohybrid of various concentrations (250, 500 µg/mL) placed in a 25 mM sodium phosphate buffer (pH-7.2) along with the control before 4 hours and incubated for 10 minutes in the dark. The whole reaction mixture (activated DCF-DA along with the LDH-IAA solution) was irradiated after 20 minutes of incubation at various pre-described times from 10-60 seconds (s) at 532 nm Laser light effectively. The resultant absorbance was measured using an Elisa reader at E_x/E_m 485/528 nm. Similarly, the free radical determination in the presence of the B16F10 cell line was performed as well as with a positive control hydrogen peroxide (H_2O_2). The assay was performed in triplicate for three independent experiments.

2.15 Cell uptake studies & fluorescence quantification using flow cytometric analysis. The drug delivery efficacy of liposome coated LDH nanoparticles (LDH-FITC-Lipo) was investigated by means of a cell uptake study using FITC conjugated LDH by visualization in BD pathway as reported previously with slight optimization.[91] B16F10 skin melanoma cells after 80% confluence were harvested with a trypsin-EDTA solution and seeded into fluorescent plates (96 well) at a density of $1x10^4$ cell/well. LDH-FITC and liposome coated LDH samples (LDH-FITC-Lipo) were incubated for 4 hours with the cells then fixed with 3.7% paraformaldehyde and eventually incubated for 10 minutes with 0.5% triton X-100 for cell wall dissociation; simultaneously 100 µL of 1% bovine serum albumin was added. The cytoskeleton and nucleus was further stained with rhodium phalloidin (100 µL, 0.05 mg/mL) and DAPI (100 µl, 0.1 mg/mL) respectively, intermittently washed thrice with PBS for each step. Eventually the cell images were captured using BD pathway.

In addition, the harvested cells were seeded in a 6 well plate at a density of $3x10^5$ cell/well, and after 24 hours of incubation the cells were treated with liposome coated LDH-FITC (100 µg/mL) in addition to the control i.e., nanoparticles devoid of FITC. Cells were collected in a tube and centrifuged at 400xg for 5 minutes, washed once with PBS and re-suspended for fluorescence quantification using flow cytometry. The samples after treatment were immediately analyzed by measuring fluorescence from the gated cell population using Beckmann coulter flow cytometry with the laser set at 530 nm in a 3 decade pulse area. The forward (FS) and side light scatter (SS) profiles were adjusted to gate for the cell population and fluorescence parameters were recorded by collecting logarithmic amplification.

2.16 Comet assay. DNA fragmentation was determined by using the most reliable technique, alkaline comet single cell

gel electrophoresis according to the manufacturer's (Trevigen) instructions. B16F10 cell lines were treated with the LDH-IAA and LDH-IAA-Lipo nanohybrids. After 4 hours of incubation, the light was irradiated for 30 seconds and further incubated for 20 hours. Cells were harvested and pooled in a 1% low melting point agarose at a ratio of 1:10 (v/v) at 37 ºC and immediately layered on custom frosted slides which feature a clear centered window. The gel was run in the alkaline electrophoresis buffer composition (0.2 N NaOH, 0.5 mM EDTA, pH-12.5) for 20 minutes at 21 Volts and 350 mA. We washed the slides in water and ethanol for 5 minutes to reanneal the DNA and finally stained the dried smear with SYBR green (1mg/mL) for 30 minutes with the micrographs captured using fluorescence image analysis.

2.17 Morphological analysis of mitochondria. Mitochondria membrane potential (MMP) was ratio metrically recognized by the indicator JC-1 stain (5,5',6,6'-tetrachloro-1,1',3,3'- tetraethyl benzimidazolyl carbocyanine iodide) observed in the cells by changes in coloration after treatment. Cultured B16F10 cell line at a density of $1x10^4$ cells/well was subjected to the treatments using LDH-IAA and LDH-IAA-Lipo under dark and light exposure. After 4 hours the light was irradiated for 30 seconds at a wavelength of 532 nm in the required wells and incubated for 20 hours. Subsequently, the indicator JC-1 stain was added at 5 µM and incubated for 30 minutes at 37 ºC. Finally, the dye was cleared off and washed twice with PBS; the cells were observed under the fluorescent microscope for dye aggregates showing different colors which represent the mitochondrial potential.

2.18 Lipid peroxidation. Lipid peroxidation is an indicator of oxidative stress. The generated thiobarbituric acid reactive substances (TBARS) such as lipid hydroperoxides and aldehydes [ex. malondialdehyde (MDA)] in the cell culture media combine with thiobarbituric acid (TBA) in a 1:2 ratio to form a fluorescent adduct. TBARS are expressed as MDA equivalents by following the procedure as reported previously.[92, 93] Cells were treated with LDH-IAA (100 µg/mL) and LDH-IAA-Lipo (100 µg/mL) and incubated for an hour besides with diethyl maleate (DEM) @ 10 mM used as a positive control. Cells from prepared flasks were harvested and seeded at a density of 5 x 10^5 cells/mL in DMEM cell culture media (2 mM L-glutamine, 10% FBS). After attaining 80% confluence after 24 hours, the cell culture media was replaced with respective test nanomaterials suspended in PBS along with negative and positive controls and incubated at 37 ºC in 5% CO_2. After 2 hours of incubation supernatant and cell lysate was extracted and the *in vitro* TBARS assay was performed. 200 µL of supernatant was taken and a mixture containing 400 µL of 0.67% TBA/0.01% BHT in 2.5% TCA and 200 µL of 15% TCA was added. This mixture was heated at 95 ºC for 30 minutes, allowed to cool down and a complex of MDA-TBA was extracted using n-butanol. Eventually, fluorescence was measured at ex. 530 nm and em. 550 nm along with the reference recoded to a reagent blank.

3. Results and discussion

The current investigations are discussed in brief. Indole acetic acid (IAA) loaded within layered double hydroxide (LDH) was synthesized and eventually coated with the biocompatible liposome using negatively charged lipids for controlled release of photosensitizer. IAA acts as a prodrug involving energy exchange phenomena through a photoreaction process when exposed to visible light. This photosensitized IAA on oxidation generates free radicals mainly (indolyl radical cation, skatolyl radical) forming reactive toxins known as highly reactive species (peroxyl radical) responsible for phototoxicity.[81] These harmful adducts obstruct seriously in the biochemical process of the cancer cell and eventually lead to death. IAA as a photosensitizer is intercalated to deliver and prove the apoptosis of skin melanoma (B16F10 cell line from mouse) under photo activation and has potential for photosensitizing capability in cancer therapy. In addition the cytocompatibility of IAA loaded nanoconstructs were tested in normal fibroblast cell line.

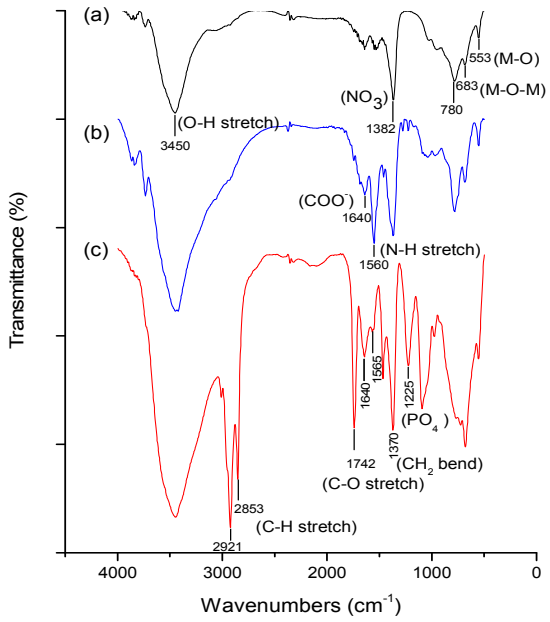

Fig. 2. FT-IR spectra of (a) pristine LDH, (b) LDH-IAA and (c) LDH-IAA-Lipo.

Fourier transform infrared (FT-IR) spectra of pristine LDH, IAA loaded LDH and liposome coated LDH are characterized and represented in Fig. 2. It infers all the molecules were stabilized after intercalation of IAA in the interlayer space of LDH with preserved functional groups. A strong and extensive band centered around 3400 cm^{-1} is the result of the O-H group stretch of absorbed water molecules and surface hydroxyl groups of LDH layered structures. A sharp peak at 1382 cm^{-1} exemplifies the interlayer nitrate ion (Fig. 2-a). The peaks at 553 and 683 cm^{-1} are attributed to the lattice vibration of M–O and M–O–M respectively,[94] These are observed on the subsequent modification of LDH which reveals the undissociative nature of LDH on modification. After the intercalation of IAA, two sharp peaks ascribed around 1560 and 1640 cm^{-1} referring to the N-H (amine) stretch and asymmetric carboxylate stretch of IAA respectively, epitomize the successful intercalation of IAA (Fig. 2-b). However an

increase in the intensities of the peak results in IAA loading although the peak at 1382 cm^{-1} reduced to some extent which shows the presence of nitrate ions in the interlayer of LDH. The coating with the lipid blend on the surface of LDH displays the absorption bands at 1370 and 1742 cm^{-1} and embodies the CH_2 bending and the C-O stretch of lecithin ester respectively. A sharp peak at 1225 cm^{-1} confirms the PO_4 stretch of lecithin and dicetyl phosphate (Fig. 2-c). However the sharp and tapered bands at 2921, 2850 cm^{-1} divulge the confirmation of the C-H stretch of cholesterol and the aliphatic hydrocarbon chain of dicetyl phosphate. These spectra clearly reveal that the LDH hasn't degraded or dissociated during the intercalation of IAA and the liposome coating on the LDH surface.

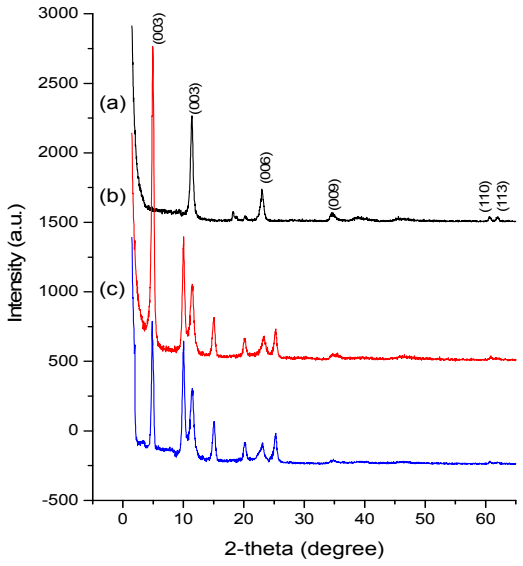

Fig. 3. Powder X-ray diffraction spectra of (a) pristine LDH, (b) LDH-IAA and (c) LDH-IAA-Lipo.

Figure 3 depicts the characteristic PXRD patterns of IAA intercalated LDH as well as liposome coated LDH. The pristine LDH has shown the characteristic diffraction peaks (2θ) at 11º, 24º and 35º which correspond to the respective planes at (003), (006) and (009) of LDH (Fig. 3-a). After the intercalation of IAA the shift in spacing of d(003) planes towards the left by an angle of 4.95 degrees and then d(006), d(009) at 10.1 and 11.4 degrees respectively (Fig. 3-b). This reveals the increase of d-spacing in d(003) to 1.79 nm after IAA intercalation from 0.82 nm (LDH) and is in clear agreement as reported previously.[95] This obviously states and supports the string of FT-IR data as determined for functional group analysis. Nevertheless the typical hexagonal structural arrangement of LDH is shown by the characteristic peaks at the planes d(110) and d(113) of the basal reflection at 60.8º and 62.2º. This arrangement facilitates the ease of the exchange process among interlayer anions without any destruction in the layered structure.[96] Moreover after coating with the liposome the changes in the PXRD pattern were negligible in the arrangement. But the d-spacing was amplified at d(003) reflection to 1.98 nm because of the geometric arrangement from the influence of electrostatic interactions between the positively charged surface of the LDH and the counter charged liposome coat (Fig. 3-c). These results could be the evidence for the LDH and its arrangement before and after the intercalation of IAA.

The thermal properties have robustly corroborated the loading efficiency and stable nature of the inorganic nanoparticle. Figure S1 represents the TGA and DTG curves of the LDH nanoparticle and its consecutive modified samples. However the degradation temperature of LDH-IAA has a shift towards the right (higher than the pristine LDH) and was reverted in the case of liposome coated LDH whereas the termination temperatures are almost similar in all cases. The stages of degradation have varied in all the samples with different thermal behavior; for instance, a well-known loss occurred because of the elimination of the absorbed interlayer water before 250 ºC. Moreover, at higher temperatures it results in the dehydroxylation of layers and the formation of double oxide-hydroxide and carbon dioxide from the layers.[97] Pristine LDH exhibited different stages of weight loss, at which the first is attributed to water loss from the surface due to physical absorption and the interlayer space of LDH nanoparticles (Fig. S1B-a). [98, 99] The next event of weight loss was followed by 28.3% of weight loss in the final stage of decomposition around 350 ºC which represents the final combustion of inorganic fractions of the nanoparticles. In LDH-IAA (Fig. S1B-b) sample, the weight loss in early stages is same as pristine LDH sample. However the final stage of the combustion profile disappeared and shifted right to 413 ºC with 45% of weight loss signifying that the drug and LDH was packed together and shrouded with layers.[95] Since drug loaded LDH nanovehicles gets degraded at higher temperatures with enhanced thermal stability supports the strength of interactions between the molecules in the interlayer gallery as well.[46] The loading of IAA was confirmed and percentage nearly matches the quantitative UV detection obtained, i.e., 19.5% (w/w) of LDH (Fig. S1A).

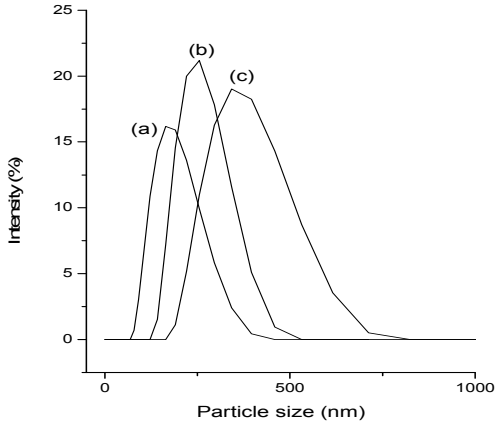

Fig. 4. Particle size distribution of (a) pristine LDH, (b) LDH-IAA and (c) LDH-IAA-Lipo.

Recently, Zhang and An co-workers have designed innovative formulations such as photosensitizer-doped perylene nanoparticles[100] as well as carrier free stable nanocrystal[101] with a very high loading percentage of the photosensitizer. These are highly effective and very

impressive in treating cancer cell. In a similar fashion using biodegradable LDH nanocarriers which has its own advantages such as surface functionalization and high surface area with controlled release property could also be supportive in preventing the instant degradation/decay of photosensitizer. In addition, these nanoconstructs are not only stable but also enhance the solubility of poorly soluble photosensitizers. In comparative to other inorganic nanocontainer like MSN with less than 5% drug loading, usage of biocompatible and biodegradable LDH with improved IAA loading efficiency (nearly 20% w/w of LDH) is beneficial. Eventually, liposome coated LDH-IAA has been subjected to TGA analysis and surprisingly the 1st event of weight loss was very less (5%), of the adsorbed water molecules until 200 ºC while the final combustion stage started at 180 ºC and lasted till 500 ºC with a weight loss of 62% (Fig. S1B-c). Since lipids are thermo sensitive organic compounds that get degraded at earlier stages, no matter the inorganic moieties which also followed at their respective temperatures at a higher combustion rate with the loss of more weight. The reduction in the degradation temperature of LDH-IAA-Lipo was evidenced by the liposome bilayer which formed a compact sheet around the positive charged layered surface of the pristine LDH. Furthermore, the degradation of LDH was extended until 450 ºC, which demonstrates the shrouded coat on the nanoparticles.

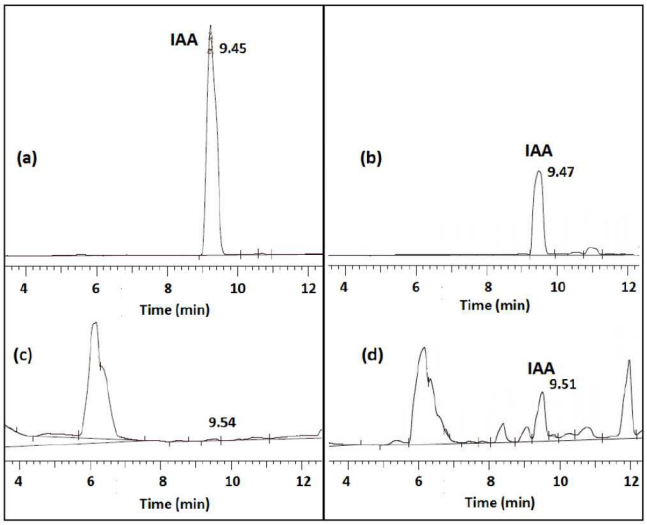

Fig. 5. Leaching/Stability test and HPLC determination representing (a) IAA alone, (b) LDH-IAA, (c) LDH-IAA-Lipo subjected to citrate buffer alone and (d) LDH-IAA-Lipo subjected to Triton X-100/Citrate buffer mixture.

The particle size measurement and the ζ-potential of various samples of LDH after modification were measured using DLS and are depicted in Fig. 4 and Table S1 respectively. The average hydrodynamic diameter of positive charged layers of pristine LDH is 167 nm (Fig. 4-a) while the potential is +47.2±0.97 mV (Table S1-a) due to magnesium and aluminium metals in the framework. The IAA loaded LDH size has been enhanced by 50 nm (Fig. 4-b) because of aggregation and the potential was drastically reduced and attained a nearly neutral state. (Table S1-b) The charge was balanced by the high loading capacity of IAA achieved by the anion exchange mechanism. This confirms the intercalation of IAA in LDH. The zeta potential measurements of all the respective samples were performed by adjusting to physiological pH-7.4. After coating with negatively charged lipids, the surface potential reduced to a large extent and terminated at -42.5 mV (Table S1-c) with the final mean hydrodynamic diameter at 320 nm (Fig. 4-c). Herewith, negatively charged lipid dicetyl phosphate was used to establish charge based interactions between positively charged layers and negatively charged lipids for a controlled release and to ensure the compactness of the coat. The thickness of the coat is not only helpful in the controlled release of IAA but also enhances the stability of the nanoparticles that assist in preventing the leaching of intercalated photosensitizer. Meanwhile this strategy offers the advantage of charge balancing capacity with negatively charged liposome at which the intercalated anions can remain stable in their respective positions from the start. Therefore, it is noteworthy that formulations with such size distribution could be established as delivery systems for various routes of administration. A stability investigation for liposome was measured by a leach test using surfactant triton X-100 (polyethylene glycol octyl phenyl ether) in citrate buffer (2:5 ratio). This creates the leakage of IAA by LDH degradation in the citrate buffer after its exposure to the wear and tear of the coat using triton X-100. Simultaneously a comparison can be made with the control i.e. exposure of LDH-IAA-Lipo using the citrate buffer alone, in which it indirectly signifies the stability of the liposome coat. However, the IAA release was highly negligible. In the HPLC determination of IAA (see in experimental section), the spectra reveals that the IAA separation is achieved at a retention time of 9.45 minutes in a 15 minutes run (Fig. 5-a). Sharp peaks were observed in the respective samples for IAA detection, which clearly shows IAA intercalation in LDH. (Fig. 5-b) The liposome coated sample (Fig. 5-d), when subjected to the triton X-100-citrate buffer mixture, leads to the disorganization of the lipid layer and eventually the LDH framework gets disintegrated after getting contact to the citrate buffer. Similarly, when the sample is subjected to treatment in the citrate buffer alone (Fig. 5-c), no peak was observed at the retention time of IAA and this represents that the coat is stable, and denotes that the LDH was encapsulated in liposome.

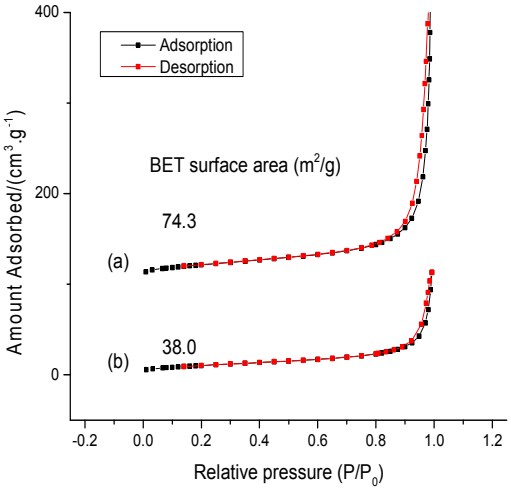

Fig. 6. Nitrogen adsorption-desorption isotherms of (a) pristine LDH and (b) LDH-IAA.

Figure S2 reveals supportive evidence for the stability study; FT-IR spectrum was recorded for the sample after being subjected to the leach test which is devoid of the N-H stretch peak of IAA at 1560 cm^{-1} and compared with the samples of LDH-IAA (Fig. S2-a), LDH-IAA-Lipo (before stability (Fig. S2-b)). This discloses the leak of IAA to a maximum extent in liposome coated LDH (Fig. S2-c). In addition, all the peaks that exemplify the LDH framework and the constituents of the liposome organization were being disturbed. These concerns can be evidenced that the liposome coat and its integrity are stronger and well established on the positive charged metal layers and helpful in the controlled delivery of the intercalated molecules. The surface area of the as-prepared LDH nanohybrids was recorded based on the nitrogen adsorption-desorption isotherms using Brunauer-Emmett-Teller (BET). The samples were degassed under a vacuum (at 80 ºC for 16 hours) prior to analysis and the results revealed a higher surface area of 74.3 $m^2.g^{-1}$ for pristine LDH (Fig. 6-a). The surface area of IAA loaded LDH shown a drastic reduction in its final surface area than the LDH alone and was recorded as 38 $m^2.g^{-1}$ (Fig. 6-b). The adsorption data represents the type IV isotherm with the hysteresis loop in the curve. Similar to the BET surface area, the pore volume was also reduced from 0.690 $cm^3.g^{-1}$ for pristine LDH to 0.175 $cm^3.g^{-1}$ for LDH-IAA. This reduction in surface area and pore volume accentuates the hybridization by intercalation of IAA in the layers of pristine LDH material. Liposome coated on LDH has shown a drastic decrease in the surface area at 1 $m^2\ g^{-1}$ (data not shown), which represents that the lipid mixture enclosed the LDH layers. This means liposome indeed has less scope to get intact with the adsorption for nitrogen which supports the liposome coating on the LDH.

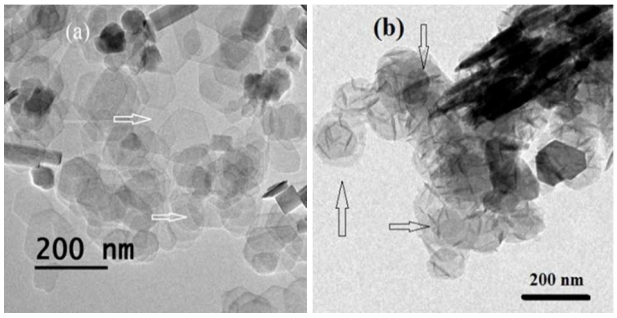

Fig. 7. TEM images (a) pristine LDH (b) LDH-IAA-Lipo.

Figure 7 illustrate the transmission electron microscopy (TEM) observations of coated and uncoated samples. As far as the size related to these micrographs are concerned, it clearly reflects that the particles are of uniform size and in proportion with the hexagonal arrangement. DLS characterized the size around 150 nm in uncoated LDH (Fig. 4-a) whereas it was double the size in the liposome coated sample (Fig. 4-c). But in the TEM we found no variation in size as a consequence of agglomeration. The liposome coated sample (Fig. 7-b) is different in comparison with the uncoated sample (Fig. 7-a) in the sense that the appearance is clumpy or misty in nature while the arrow represents the hexagonal shape of the LDH on the left (Fig. 7-a) and the layer of coating on the surface of LDH in the right image (Fig. 7-b). These hexagonal plate like structures are clear in view and after intercalation and coating, some of them turned to nanorods by agglomeration or were further modified due to crystal growth.[89] TEM observation individualized the morphology of nanoparticles before and after coating which are partially clustered and within the size range of around 100 nm.

An IAA cumulative release study from LDH nanohybrids was performed in the simulated body fluids at pH 5.0 and 7.4 to mimic *IVIVC* (*in vitro-in vivo* correlation). It was not conducted in pH-1.2 (0.1M HCl) because of the LDH instability in acidic environments. The release curves of the drug intercalated LDH nanohybrids in pH- 5.0, 7.4 (PBS) indicate the burst release mechanism in both the environments due to the high exchange capacity of IAA at around 90% in first 3 hours. Similar circumstances were provided for the samples coated with liposome. In addition, the test was also performed in a pH-1.2 buffer.

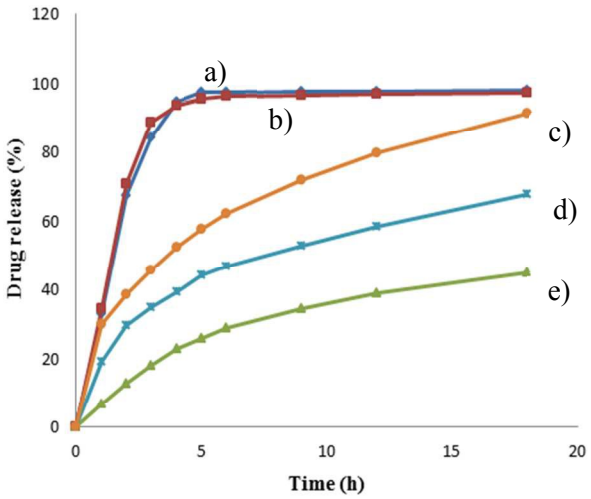

Fig. 8. IAA release from LDH and LDH-IAA-Lipo samples at various time intervals in physiological simulated fluids (PBS) (a) LDH-IAA in pH-5.0 (b) LDH-IAA at 7.4 (c) LDH-IAA-Lipo at pH-7.4. (d) LDH-IAA-Lipo at pH-5.0. (e) LDH-IAA-Lipo at pH-1.2

The release rates of all the samples are depicted in the Fig. 8 with the plots of percentage drug release against time. However the controlled release behavior in the respective buffers was attained by the interlocking of lipids in the liposome coat around the LDH. The release is approximately 70 and 90% in pH 5.0 (nearly skin pH) and 7.4 respectively. The metal hydroxide layer in the lipid was more stable in these buffers and facilitated good ion-exchange capacity at which the IAA release ended conveniently. The highest amount of drug release was achieved because of its ample solubility in alkaline pH. However this surprising and controlled behavior even ensued at pH-5.0 because of the liposome coat, since the disintegration of the inorganic host was prevented which is characterized by the arrest of the IAA intercalated LDH inside the liposome coat. Such a discrepancy is possible because of the release exchange mechanism of the interlayer ions and the integrity of the lipids in the liposome anticipated for sustained delivery was satisfactory. This is in contrast to pH-1.2 where the release was very low (nearly 40%) compared to other buffers because the liposome is stable in acidic pH. This kind of optimized release behavior could help the delivery system for a controlled release of IAA for PDT.

Cellular internalization of nanocontainers was visualized by fluorescent tags immobilized with amine linkage on the LDH surface. The surface amination was confirmed by the ninhydrin reagent, the most common method of detecting primary amines. The UV-Vis absorption spectrum of all the LDH samples on successive modification at 580 nm after being subjected with ninhydrin reagent displayed in Fig. S3. Among all the samples, LDH-NH_2 alone has displayed a strong band and is devoid of the same in all the others. It is evident from the inset figure that the tubes display positive confirmation for ninhydrin.

a) b)

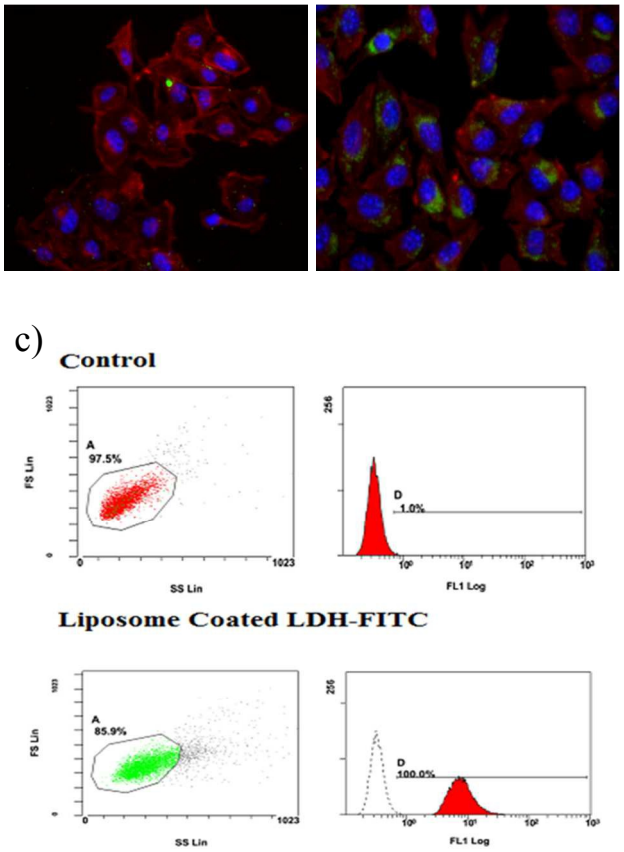

Fig. 9. Cell uptake study i.e., images captured using BD pathway represent nuclei stained with DAPI (blue) and cytoskeletons in rhodium Phalloidin (red) of (a) LDH-NH-FITC (b) LDH-NH-FITC-Lipo in green, respectively (c) Flow cytometric quantification of fluorescence using liposome coated LDH-NH-FITC (100 µg/mL) compared with control (devoid of nanoparticles) in B16F10 cell line.

Primary amines on LDH surfaces generate Ruhemann's purple coloration when heated (Fig. S3-c). However, it is devoid of the color before modification (Fig. S3-b) and after conjugation with FITC (Fig. S3-d) as well as liposome coated samples (Fig. S3-e). The disappearance of purple coloration in FITC modified samples of LDH validates the complete conjugation of the FITC molecules, as ninhydrin is known to be inactive for secondary amine of the LDH-NH-FITC molecules. Recently, many groups have studied the cellular uptake of uncoated inorganic nanoparticles[91, 102-106] that are size dependent since the internalization of these nanovehicles is challenging due to their increasing size after aggregation. This cellular uptake (internalization) plays an important role in the efficient delivery with respect to activity of photosensitizer from the nanoparticle.[4, 102] However the advantage of the liposome coated nanoparticles (LDH-NH-FITC-Lipo) is that they are tuned to establish the ease of internalization in a comfortable way and thus prove that the liposome coated systems are size and charge independent. The uptake study of uncoated nanohybrid (LDH-NH-FITC) was observed concurrently at which lesser amounts of green fluorescence was seen inside the cell that might correspond to the aggregation encountered which embodies the naked LDH. Additionally, flow cytometric analysis is performed for the quantification

of the fluorescence inside the cell; Figure 9-c reveals the maximum internalization at 85% confluence of the cells gated in comparison with the control in the B16F10 cell line. Adherent fluorescence was not observed and successful cellular internalization was achieved because of the coating of lipids to the nanoparticle surface which doesn't have any influence on charge interactions on the cell line surface even after 24 hours of incubation.

Free radicals are a kind of the most reactive species measured by using non-specific chemiluminescent dye called 2',7'-dichlorodihydrofluorescein-diacetate (H_2DCF-DA) assay. The scavenging capacity was determined by measuring the DCF (dichlorofluorescein), the oxidized form of DCFDA, which correlates the amount of free radicals generated on light irradiation. Furthermore the higher levels of free radicals generated can damage the cellular constituents and are responsible for cytotoxicity. To demonstrate the IAA can produce free radicals under light irradiation, we treated DCFDA with LDH-IAA in PBS buffer. With successive increase of the time of light exposure, a simultaneous increase in the amount of free radical generation was observed (Fig. S4-a). However, after 30 seconds, the plateau was attained by increasing the exposure time and finally this optimized unit was fixed as the effective time period for PDT and further cytotoxic studies were continued. Anti-cancerous activity is completely dependent on the amount of light energy abounding in cell oriented studies. For the liposome-coated LDH-IAA sample, the lipid membranes may affect the addition reaction of free radicals and DCFDA; and therefore, a quantitative result didn't show in our data. Previously, a study has revealed that anti-microbial activity with activated IAA by using UV-light and visible light; however it was the first time using photosensitizer IAA against a skin melanoma cell line.[78] The *in vitro* generation (devoid of cell line) of free radicals by the released IAA from the LDH was higher on exposure to the visible light for a span of 30 seconds (Fig. S4-b). It is clear from the graph that the free radical scavenging/fluorescence are neither achieved only by light nor DCFDA but by a blend of the two.[78] The influence of the nanoparticle in delivering the photosensitizer can be understood from Fig. S4-b, where the free radicals generated by an equivalent amount of IAA are less than the IAA intercalated nanovehicle. Because LDH enhances the drug solubility[107] with high carrying capacity and eventual photodynamic therapy, free radical generation and *in vitro* anti-cancerous activity was continued with the same light irradiation time.

b)

a)

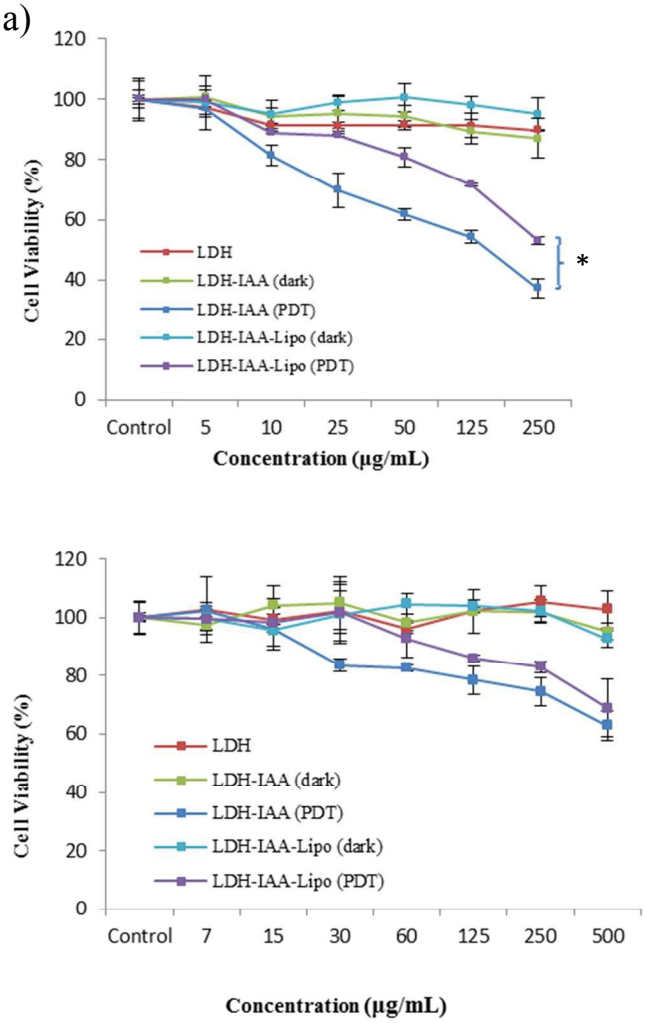

Fig. 10. Cell viability (MTT assay) of LDH, LDH-IAA LDH-IAA-Lipo at increasing concentrations, (a) In mouse melanoma (B16F10) cell line (0-250 µg/mL), (b) In normal fibroblast (3T3) cell line (0-500 µg/mL), in presence and absence of light irradiation (532 nm).* represents $p<0.001$ (one way ANOVA using Tukey test) for all the three curves.

Since IAA acts as a prodrug by generating reactive oxygen species (ROS) involving energy exchange through a photoreaction process when exposed to visible light harmless to the human body. Eventually the ability of generated ROS to damage cellular components that leads to cell death. This is possibly due to intrinsically increased oxidative stress and susceptibility to free radical assaults. This is evident from the intracellular ROS measured by DCFDA assay when compared with the positive control H_2O_2. IAA in the presence of light has generated more ampoule fluorescence than the dark which is almost comparable to the H_2O_2 in both the samples of LDH-IAA and LDH-IAA-Lipo. (Fig. S4-c). Light irradiation time and area of exposure should be necessarily taken into account while treating the patient with skin cancer; however laser light in the visible region around 532 nm is not that harmful. In contrast to the other photosensitizers, it could be established as a potential drug with no adverse effects when activated using light in the visible range. These results have proved that IAA itself acts as a free radical

generator and gets accumulated in cells which provide a strong substantiation for anti-cancer activity with photodynamic therapy on melanoma cell line.

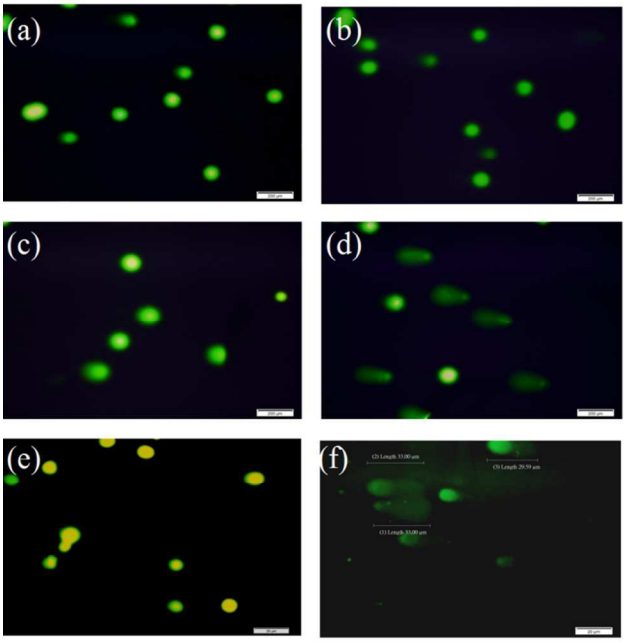

Fig. 11. DNA fragmentation was detected by single cell gel electrophoresis (Comet assay); (a) control in dark (b) control in presence of light for 30 seconds (c) LDH-IAA in dark (250 µg/mL), (d) LDH-IAA in presence of light (250 µg/mL), (e) LDH-IAA-Lipo in dark (250 µg/mL) and (f) LDH-IAA-Lipo in presence of light (250 µg/mL). Nucleic acid was stained by SYBR green. Scale bar-20 µm.

Cell proliferation studies were performed by a MTT assay (Fig. 10-a) in the mouse melanoma (B16F10) cell line. The rationale behind choosing the B16F10 cell line is because the activated IAA compound on delivery acts as a photosensitizer which is efficient in proving surface photo dynamic therapy. These experiments were designed using various conditions such as the PDT effect of IAA determined by using bare as well as liposome coated LDH nanoconstructs in the presence and absence of light. The activity of the delivered photosensitizer against the B16F10 cell line was decreased in accordance with the concentration and the difference was significant across the range of 250 µg/mL. But in contrast, the LDH alone as well as other nanoparticles (both LDH-IAA and LDH-IAA-Lipo) in the dark seems to be inactive even at higher concentrations. On augmentation of the time for irradiation of light (Fig. S4-d), it was apparent that activation as well as anti-cancer activity of IAA was proportionate in both liposome coated as well as uncoated LDH nanoconstructs.

In a normal fibroblast cell line, surprisingly liposome coated and uncoated LDH-IAA (PDT) at 500 µg/mL (Fig. 10-b) resulted in more viable cells than in a melanoma cell line (LDH-IAA (PDT) and LDH-IAA-Lipo (PDT) @ 250 µg/mL (Fig. 10-a)). This confirms the cytocompatibility nature of layered nanoconstructs under irradiation in normal fibroblasts cell line. The remaining samples (LDH, LDH-IAA and LDH-IAA-Lipo in the dark) had shown similar results as in the B16F10 cell line. The reason behind this surprise is the greater abridged uptake of nanoparticles by normal fibroblast than cancer cells.[108]

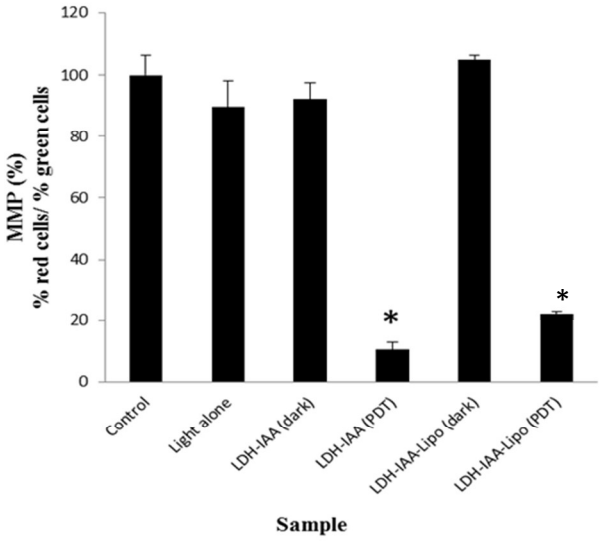

Fig. 12. Graphical representation for quantification of the J aggregates (Mitochondria membrane potential using JC-1 stain) analyzed at respective emission wavelength regions of red and green fluorescence using different conditions of LDH-IAA @ 250 µg/mL and LDH-IAA-Lipo @ 250 µg/mL. The values are represented as the mean±SD of three individual experiments. Statistical significance between treated and control is denoted by * ($p<0.001$) using a one way ANOVA (Tukey test).

Intracellular free radicals generated on irradiation are likely one of the possible causes of the cell death by destabilizing cell functions and cell metabolism with morphologic and biochemical changes typical in apoptosis. Therefore we infer that the IAA is delivered from the LDH nanovehicle after its successful uptake by endocytosis, and on activation with the light it tends to act inside the cell. A delivery system with a liposome coat around the LDH layers facilitates the delayed release of photosensitizer, which also favors the LDH nanoparticle's cell uptake mechanism. These results represent that the activated IAA in the presence of green light (532 nm) could act as a treatment option for the delivery of a potent anticancer agent specifically designed for skin related cancers when PDT has been suggested. However programmed cell death was confirmed by the DNA fragmentation study using the comet assay. DNA damage/fragmentation associated after oxidative stress smash up was visualized using an alkaline comet assay by staining the nucleic acid using SYBR green (Fig. 11). There was a significant amount of DNA damage in cells treated with IAA immobilized LDH (Fig. 11-d) as well as liposome coated LDH nanocontainers (Fig. 11-f) on irradiation of light for 30 seconds. When compared with the control experiments (Fig. 11-a), we have verified that the comet with the treatment of light (Fig. 11-b) and drug loaded nanoparticles alone (Fig. 11-c), inflict no significant damage on the DNA. This exhibited a supercoiled compact DNA without any transformation that represents that light alone cannot affect the DNA too. This typically reveals that the free radicals generated from the activated form of IAA

on exposure to light, eventually are responsible for their fragmentation with elongated tails. However it was a characteristic move that the uncoiled and damaged DNA was broken into fragments representing the photodynamic ability of free radicals generated by IAA in the B16F10 cell line.

Apoptosis was virtually visualized by means of mitochondrial membrane potential (MMP) loss performed using the vital cationic carbocyanine dye, the sensitive marker JC-1. It is one of the tools for detecting cell death by fluorescence emitted. This is exhibited as a monomer at low concentrations and yields a green fluorescence which looks similar to fluorescein in a depolarized state i.e. dead cells.[109] In the hyperpolarization state, the dye aggregates preferentially in the mitochondria by a Δψ-dependent mechanism and fluoresce red as seen in the healthy cells i.e. the control in dark (Fig. S5-a), control in light (Fig. S5-b), LDH-IAA in dark (Fig. S5-c) and LDH-IAA-Lipo in dark (Fig. S5-e). In contrast, the treated cells underwent depolarization because of cell apoptosis due to the free radical attack of IAA in the cytosol on light irradiation. Since it is an execution of apoptosis as pro-apoptotic signals generated by the caspase family of proteins,[110] the alterations in the mitochondria are due to the permeabilization of the outer mitochondrial membrane and the consequent release of apoptotic proteins.

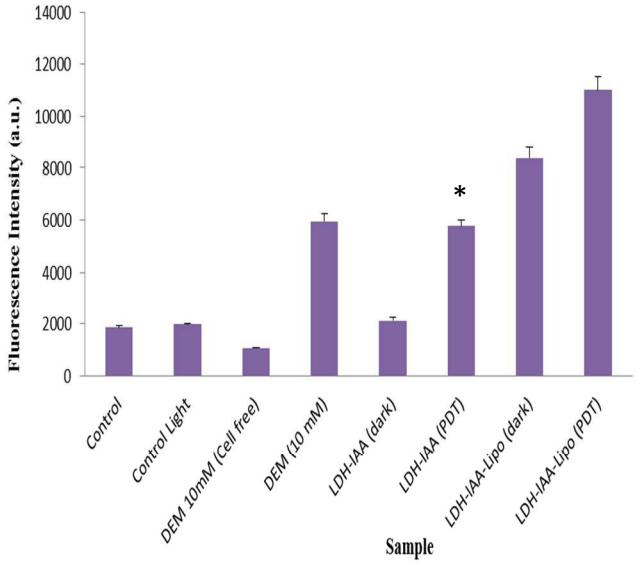

Fig. 13. Lipid peroxidation determined using a TBARS assay of LDH-IAA and LDH-IAA-Lipo (both treated @ 100 µg/mL). Diethyl maleate (DEM) is the positive control @ 10 mM concentration compared in the absence of the B16F10 cell line. The values are represented as the mean±SD of three individual experiments. Statistical significance between treated and control is denoted by * ($p<0.001$) using a one way ANOVA (Tukey test)

In addition, the loss of the electrochemical gradient, which is regulated by the respective mechanism inside the cell, is central to the apoptotic pathway.[111] Eventually, it was clear that the IAA from LDH (Fig. S5-d) as well as LDH-Lipo (Fig. S5-f) in the presence of light gets activated and the green fluorescence is dominant with depolarization levels. This represents the damage of the mitochondrial membrane that maintains the electrochemical gradient (Fig. 12). In comparison, it was not that active when applied with light and the drug individually. This kind of approach reflects the combinatorial therapy.

Oxidative deterioration of the cell membrane lipids was measured using an MDA: TBA adduct formed by the lipid peroxidation which occurred during free radical generation which causes subsequent cell cycle alteration and cell death.[112] This can be correlative data for fatty peroxide formation and the bursting out of the cell wall. The underlying mechanism involved in the detection of lipid peroxidation was the formation of malondialehyde on the deterioration of the conjugated dienes in the cell membrane which acts as an index. The generation of the malondialdehyde levels of LDH-IAA as shown in Fig. 13. At the respective concentration of LDH-IAA and in the absence of light irradiation, the MDA levels are almost equaled to the control, besides while light alone did not have any effect on the cell line. Liposome coated samples of LDH-IAA have generated higher MDA levels during detection since the lecithin (one of the substituents of liposome coat) is unsaturated. This interfere in the absorbance of MDA-TBA adduct during lipid peroxidation because the formulation surprisingly shown higher MDA levels of LDH-IAA-Lipo in dark. Eventually the result of LDH-IAA correlates to the subsequent generation of free radicals in the presence of light, which was the most likely cause of cancer cell death.

4. Conclusions

In summary, we have formulated a delivery system suitable for the controlled delivery of non-cytotoxic photosensitizer (IAA) loaded nanocontainer (LDH) coated with liposome for therapy against skin melanoma. These biodegradable and biocompatible LDH nanoconstructs are active in the presence of laser light in the visible region (532 nm). Liposome coated nanohybrids are advantageous over conventional dosage systems in their controlled release behavior with significant improvement in surface area and the highest carrying capacity. The mechanism underlying the IAA cytotoxicity in treating skin melanoma was the photo activation phenomenon. In order to prove this, we performed cell activity based assays and cell uptake studies as well as mitochondria membrane potential which is responsive to PDT. These findings could suggest to the researchers that photodynamic therapy is one of the most useful techniques in drug therapy, and the liposome coated LDH nanocontainers could serve as the best systems for sustained delivery of various drugs including photosensitizers. This system using nano-photosensitizer shows a great promise in melanoma phototherapy.

Acknowledgements

We are thankful to the Ministry of Science and Technology (MOST), Taiwan for research grants (NSC 101-2113-M-259-003-MY2, MOST 103-2113-M-259-005-MY2).

References

1. V. Saranga-Perry, C. Ambe, J. S. Zager and R. R. Kudchadkar, *CA: A Cancer Journal for Clinicians*, 2014, 64, 171-185.

2. V. Gray-Schopfer, C. Wellbrock and R. Marais, *Nature*, 2007, 445, 851-857.
3. D. Kessel, *Photodiagnosis and Photodynamic Therapy*, 2004, 1, 3-7.
4. R. R. Allison, G. H. Downie, R. Cuenca, X.-H. Hu, C. J. H. Childs and C. H. Sibata, *Photodiagnosis and Photodynamic Therapy*, 2004, 1, 27-42.
5. D. E. Dolmans, D. Fukumura and R. K. Jain, *Nature reviews. Cancer*, 2003, 3, 380-387.
6. S. K. Pushpan, S. Venkatraman, V. G. Anand, J. Sankar, D. Parmeswaran, S. Ganesan and T. K. Chandrashekar, *Current medicinal chemistry. Anti-cancer agents*, 2002, 2, 187-207.
7. P. Juzenas, R. Sørensen, V. Lani and J. Moan, *Photochemistry and photobiology*, 1999, 69, 478-481.
8. T. J. Dougherty, C. J. Gomer, B. W. Henderson, G. Jori, D. Kessel, M. Korbelik, J. Moan and Q. Peng, *Journal of the National Cancer Institute*, 1998, 90, 889-905.
9. K. R. Weishaupt, C. J. Gomer and T. J. Dougherty, *Cancer Research*, 1976, 36, 2326-2329.
10. L. Minai, D. Yeheskely-Hayon and D. Yelin, *Scientific reports*, 2013, 3, 2146.
11. S. H. Ibbotson, *The British journal of dermatology*, 2002, 146, 178-188.
12. S. B. Brown, E. A. Brown and I. Walker, *The Lancet Oncology*, 2004, 5, 497-508.
13. G. Serša, B. Štabuc, M. Čemažar, D. Miklavčič and Z. Rudolf, *Clinical Cancer Research*, 2000, 6, 863-867.
14. W. Sun and L. Schuchter, *Curr. Treat. Options in Oncol.*, 2001, 2, 193-202.
15. G. B. Kharkwal, S. K. Sharma, Y. Y. Huang, T. Dai and M. R. Hamblin, *Lasers in surgery and medicine*, 2011, 43, 755-767.
16. L. N. M. Ribeiro, A. C. S. Alcântara, M. Darder, P. Aranda, F. M. Araújo-Moreira and E. Ruiz-Hitzky, *International journal of pharmaceutics*, 2014, 463, 1-9.
17. S. Bhattacharyya, R. A. Kudgus, R. Bhattacharya and P. Mukherjee, *Pharmaceutical research*, 2011, 28, 237-259.
18. Z. Hu and G. Chen, *RSC Advances*, 2013, 3, 12021-12025.
19. A. I. Khan and D. O'Hare, *Journal of Materials Chemistry*, 2002, 12, 3191-3198.
20. X. Wu, H. Li, S. Song, R. Zhang and W. Hou, *International journal of pharmaceutics*, 2013, 454, 453-461.
21. X. Pang, X. Ma, D. Li and W. Hou, *Solid State Sciences*, 2013, 16, 71-75.
22. L. Dong, L. Yan, W.-G. Hou and S.-J. Liu, *Journal of Solid State Chemistry*, 2010, 183, 1811-1816.
23. S. Mallakpour, M. Dinari and V. Behranvand, *RSC Advances*, 2013, 3, 23303-23308.
24. V. R. L. Constantino and T. J. Pinnavaia, *Inorganic Chemistry*, 1995, 34, 883-892.
25. W.-G. Hou and Z.-L. Jin, *Colloid Polym Sci*, 2007, 285, 1449-1454.
26. J.-H. Choy, S.-J. Choi, J.-M. Oh and T. Park, *Applied Clay Science*, 2007, 36, 122-132.
27. V. Rives, M. del Arco and C. Martín, *Applied Clay Science*, 2014, 88–89, 239-269.
28. S. Anandan, C.-Y. Chen and J. J. Wu, *RSC Advances*, 2014, 4, 55519-55523.
29. M. de Victoria Rodriguez, E. Brunet, M. Nocchetti, F. Presciutti and F. Costantino, *RSC Advances*, 2014, 4, 26912-26917.
30. U. Costantino, M. Nocchetti, L. Tammaro and V. Vittoria, *Recent patents on nanotechnology*, 2012, 6, 218-230.
31. L. Perioli and C. Pagano, *Expert Opin Drug Deliv*, 2012, 9, 1559-1572.
32. E. Conterosito, W. Van Beek, L. Palin, G. Croce, L. Perioli, D. Viterbo, G. Gatti and M. Milanesio, *Crystal Growth & Design*, 2013, 13, 1162-1169.
33. T. Selvam, A. Inayat and W. Schwieger, *Dalton Transactions*, 2014, 43, 10365-10387.
34. H. Li, J. Wen, R. Yu, J. Meng, C. Wang, C. Wang and S. Sun, *RSC Advances*, 2014, DOI: 10.1039/C4RA15395B.
35. B. Yang and Z. Yang, *RSC Advances*, 2013, 3, 12589-12592.
36. K. Xu, Z. Zhang, G. Chen and J. Shen, *RSC Advances*, 2014, 4, 19218-19220.
37. Y. Li, W.-G. Hou and W.-Q. Zhu, *Colloids and Surfaces A: Physicochemical and Engineering Aspects*, 2007, 303, 166-172.
38. Z. Zhang, G. Chen and J. Liu, *RSC Advances*, 2014, 4, 7991-7997.
39. M. Zhang, B. Gao, J. Fang, A. E. Creamer and J. L. Ullman, *RSC Advances*, 2014, 4, 28171-28175.
40. Y. Wang, Y. Zhou, T. Zhang, M. He and X. Bu, *RSC Advances*, 2014, 4, 29968-29974.
41. K. Ladewig, Z. P. Xu and G. Q. Lu, *Expert Opinion on Drug Delivery*, 2009, 6, 907-922.
42. Z. P. Xu, M. Niebert, K. Porazik, T. L. Walker, H. M. Cooper, A. P. J. Middelberg, P. P. Gray, P. F. Bartlett and G. Q. Lu, *Journal of Controlled Release*, 2008, 130, 86-94.
43. J. M. Oh, C. B. Park and J. H. Choy, *Journal of nanoscience and nanotechnology*, 2011, 11, 1632-1635.
44. U. Riaz and S. M. Ashraf, *Mini reviews in medicinal chemistry*, 2013, 13, 522-529.
45. S. J. Choi, J. M. Oh, H. E. Chung, S. H. Hong, I. H. Kim and J. H. Choy, *Current pharmaceutical design*, 2013, 19, 7196-7202.
46. J. H. Choy, J. S. Jung, J. M. Oh, M. Park, J. Jeong, Y. K. Kang and O. J. Han, *Biomaterials*, 2004, 25, 3059-3064.
47. S. Yan, B. E. Rolfe, B. Zhang, Y. H. Mohammed, W. Gu and Z. P. Xu, *Biomaterials*, 2014, 35, 9508-9516.
48. L. Li, W. Gu, J. Chen, W. Chen and Z. P. Xu, *Biomaterials*, 2014, 35, 3331-3339.
49. R. Liang, M. Wei, D. G. Evans and X. Duan, *Chem Commun (Camb)*, 2014, 50, 14071-14081.
50. K. Ladewig, M. Niebert, Z. P. Xu, P. P. Gray and G. Q. M. Lu, *Biomaterials*, 2010, 31, 1821-1829.
51. A. S. Thakor and S. S. Gambhir, *CA: A Cancer Journal for Clinicians*, 2013, 63, 395-418.
52. S. Nazir, T. Hussain, A. Ayub, U. Rashid and A. J. MacRobert, *Nanomedicine: Nanotechnology, Biology and Medicine*, 2014, 10, 19-34.
53. K. H. Bae, H. J. Chung and T. G. Park, *Molecules and cells*, 2011, 31, 295-302.
54. D. Banerjee, R. Harfouche and S. Sengupta, *Vascular cell*, 2011, 3, 3.
55. Z. P. Xu and G. Q. Lu, *Pure Appl Chem*, 2006, 78, 1771-1779.
56. D. Carriazo, M. del Arco, C. Martín, C. Ramos and V. Rives, *Microporous and Mesoporous Materials*, 2010, 130, 229-238.
57. J. H. Choy, S. Y. Kwak, J. S. Park, Y. J. Jeong and J. Portier, *Journal of the American Chemical Society*, 1999, 121, 1399-1400.
58. L. Qin, M. Wang, R. Zhu, S. You, P. Zhou and S. Wang, *International journal of nanomedicine*, 2013, 8, 2053-2064.
59. Z. Gu, A. C. Thomas, Z. P. Xu, J. H. Campbell and G. Q. Lu, *Chemistry of Materials*, 2008, 20, 3715-3722.
60. M. S. Gasser, *Colloids and surfaces. B, Biointerfaces*, 2009, 73, 103-109.
61. M. del Arco, A. Fernández, C. Martín and V. Rives, *Applied Clay Science*, 2009, 42, 538-544.
62. S.-J. Ryu, H. Jung, J.-M. Oh, J.-K. Lee and J.-H. Choy, *Journal of Physics and Chemistry of Solids*, 2010, 71, 685-688.
63. R. Rojas, A. F. Jimenez-Kairuz, R. H. Manzo and C. E. Giacomelli, *Colloids and Surfaces A: Physicochemical and Engineering Aspects*, 2014, 463, 37-43.

64. S. S. Yoo, R. Razzak, E. Bedard, L. Guo, A. R. Shaw, R. B. Moore and W. H. Roa, *Nanotechnology*, 2014, 25, 425102.
65. Z. L. Liu, D. Y. Tian, S. P. Li, X. D. Li and T. H. Lu, *International journal of pharmaceutics*, 2014, 473, 414-425.
66. D. Dorniani, M. Z. Hussein, A. U. Kura, S. Fakurazi, A. H. Shaari and Z. Ahmad, *Drug design, development and therapy*, 2013, 7, 1015-1026.
67. Z. P. Xu, T. L. Walker, K. L. Liu, H. M. Cooper, G. Q. Lu and P. F. Bartlett, *International journal of nanomedicine*, 2007, 2, 163-174.
68. B. Saifullah, M. Z. Hussein, S. H. Hussein-Al-Ali, P. Arulselvan and S. Fakurazi, *Drug design, development and therapy*, 2013, 7, 1365-1375.
69. C. E. Ashley, E. C. Carnes, K. E. Epler, D. P. Padilla, G. K. Phillips, R. E. Castillo, D. C. Wilkinson, B. S. Wilkinson, C. A. Burgard, R. M. Kalinich, J. L. Townson, B. Chackerian, C. L. Willman, D. S. Peabody, W. Wharton and C. J. Brinker, *ACS nano*, 2012, 6, 2174-2188.
70. J. Liu, X. Jiang, C. Ashley and C. J. Brinker, *Journal of the American Chemical Society*, 2009, 131, 7567-7569.
71. A. Laouini, C. Jaafar-Maalej, I. Limayem-Blouza, S. Sfar, C. Charcosset and H. Fessi, *Journal of Colloid Science and Biotechnology*, 2012, 1, 147-168.
72. R. Liu, L. Gan, X. Yang and H. Xu, *Journal of bioscience and bioengineering*, 2011, 111, 98-103.
73. W. Sun, N. Zhang, A. Li, W. Zou and W. Xu, *International journal of pharmaceutics*, 2008, 353, 243-250.
74. M. Merchan, T. S. Ouk, P. Kubat, K. Lang, C. Coelho, V. Verney, S. Commereuc, F. Leroux, V. Sol and C. Taviot-Gueho, *Journal of Materials Chemistry B*, 2013, 1, 2139-2146.
75. K. Lang, P. Bezdička, J. L. Bourdelande, J. Hernando, I. Jirka, E. Káfuňková, F. Kovanda, P. Kubát, J. Mosinger and D. M. Wagnerová, *Chemistry of Materials*, 2007, 19, 3822-3829.
76. J. I. Na, S. Y. Kim, J. H. Kim, S. W. Youn, C. H. Huh and K. C. Park, *Lasers in surgery and medicine*, 2011, 43, 200-205.
77. S. Y. Huh, J. I. Na, C. H. Huh and K. C. Park, *Annals of dermatology*, 2012, 24, 56-60.
78. S. Y. Kim, J. S. Ryu, H. Li, W. J. Park, H. Y. Yun, K. J. Baek, N. S. Kwon, U. D. Sohn and D. S. Kim, *Anticancer research*, 2010, 30, 4607-4612.
79. P. Wardman, *Current pharmaceutical design*, 2002, 8, 1363-1374.
80. L. P. Candeias, L. K. Folkes, M. F. Dennis, K. B. Patel, S. A. Everett, M. R. L. Stratford and P. Wardman, *The Journal of Physical Chemistry*, 1994, 98, 10131-10137.
81. L. K. Folkes and P. Wardman, *Cancer Research*, 2003, 63, 776-779.
82. K. C. Park, S. Y. Kim and D. S. Kim, *Biological & pharmaceutical bulletin*, 2009, 32, 1609-1613.
83. D. S. Kim, S. Y. Kim, Y. M. Jeong, S. E. Jeon, M. K. Kim, S. B. Kwon, J. I. Na and K. C. Park, *Biological & pharmaceutical bulletin*, 2006, 29, 2404-2409.
84. S. Y. Kim, M. K. Kim, S. B. Kwon, J. I. Na, K. C. Park and D. S. Kim, *Archives of dermatological research*, 2009, 301, 319-322.
85. Z. P. Xu, G. Stevenson, C. Q. Lu and G. Q. Lu, *The journal of physical chemistry. B*, 2006, 110, 16923-16929.
86. J.-M. Oh, S.-J. Choi, G.-E. Lee, S.-H. Han and J.-H. Choy, *Adv Funct Mater*, 2009, 19, 1617-1624.
87. Z. P. Xu, G. S. Stevenson, C.-Q. Lu, G. Q. Lu, P. F. Bartlett and P. P. Gray, *Journal of the American Chemical Society*, 2006, 128, 36-37.
88. A. M. Fogg, J. S. Dunn, S.-G. Shyu, D. R. Cary and D. O'Hare, *Chemistry of Materials*, 1998, 10, 351-355.
89. P.-R. Wei, S.-H. Cheng, W.-N. Liao, K.-C. Kao, C.-F. Weng and C.-H. Lee, *Journal of Materials Chemistry*, 2012, 22, 5503-5513.
90. T. Mosmann, *Journal of immunological methods*, 1983, 65, 55-63.
91. F. Lu, S. H. Wu, Y. Hung and C. Y. Mou, *Small*, 2009, 5, 1408-1413.
92. W. Q. Ding, B. Liu, J. L. Vaught, R. D. Palmiter and S. E. Lind, *Molecular cancer therapeutics*, 2006, 5, 1864-1872.
93. W. G. Niehaus, Jr. and B. Samuelsson, *European journal of biochemistry / FEBS*, 1968, 6, 126-130.
94. J. Theo Kloprogge and R. L. Frost, *Applied Catalysis A: General*, 1999, 184, 61-71.
95. S. H. Hussein Al Ali, M. Al-Qubaisi, M. Z. Hussein, M. Ismail, Z. Zainal and M. N. Hakim, *International journal of nanomedicine*, 2012, 7, 4251-4262.
96. H. Zhang, D. Pan, K. Zou, J. He and X. Duan, *Journal of Materials Chemistry*, 2009, 19, 3069-3077.
97. S. Velu, K. Suzuki, M. Okazaki, T. Osaki, S. Tomura and F. Ohashi, *Chemistry of Materials*, 1999, 11, 2163-2172.
98. J.-H. Yang, Y.-S. Han, M. Park, T. Park, S.-J. Hwang and J.-H. Choy, *Chem Mater*, 2007, 19, 2679-2685.
99. Z. Wang, E. Wang, L. Gao and L. Xu, *J Solid State Chem*, 2005, 178, 736-741.
100. J. Zhang, F. An, Y. Li, C. Zheng, Y. Yang, X. Zhang and X. Zhang, *Chemical communications*, 2013, 49, 8072-8074.
101. F.-F. An, Y. Li and J. Zhang, *Materials Letters*, 2014, 122, 323-326.
102. Z. P. Xu, Q. H. Zeng, G. Q. Lu and A. B. Yu, *Chemical Engineering Science*, 2006, 61, 1027-1040.
103. J. M. Oh, S. J. Choi, S. T. Kim and J. H. Choy, *Bioconjugate chemistry*, 2006, 17, 1411-1417.
104. J. M. Oh, S. J. Choi, G. E. Lee, J. E. Kim and J. H. Choy, *Chemistry, an Asian journal*, 2009, 4, 67-73.
105. S. J. Choi and J. H. Choy, *Nanomedicine*, 2011, 6, 803-814.
106. S.-J. Choi and J.-H. Choy, *Nanomedicine*, 2011, 6, 803-814.
107. T.-H. Kim, G. J. Lee, J.-H. Kang, H.-J. Kim, T.-i. Kim and J.-M. Oh, *BioMed Research International*, 2014, 2014, 11.
108. R. Ma, Z. Wang, L. Yan, X. Chen and G. Zhu, *Journal of Materials Chemistry B*, 2014, 2, 4868-4875.
109. J. D. Ly, D. R. Grubb and A. Lawen, *Apoptosis*, 2003, 8, 115-128.
110. N. Zamzami and G. Kroemer, *Current Biology*, 2003, 13, R71-R73.
111. J. D. Ly, D. R. Grubb and A. Lawen, *Apoptosis : an international journal on programmed cell death*, 2003, 8, 115-128.
112. M. A. Tirmenstein, F. A. Nicholls-Grzemski, J. G. Zhang and M. W. Fariss, *Chemico-biological interactions*, 2000, 127, 201-217.